International Journal of ChemTech Research
CODEN (USA): IJCRGG ISSN: 0974-4290
Vol.8, No.9 pp 456-468, 2015

# Electrosynthesis, Characterization and Performance of Pt–Sn–Rh/C catalyst for Methanol Oxidation

**S.M. Nayeemunisa[1,3], S. Kiruthika[2], K. Ponmani[3], M.Elumalai[3] and B. Muthukumaran[3]***

[1]Department of Chemistry, Justice Basheer Ahmed Sayeed College for Women, Chennai – 600 018, India.
[2]Department of Chemical Engineering, SRM University, Chennai – 603 203, India.
[3]Department of Chemistry, Presidency College, Chennai – 600 005, India.

**Abstract:** A systematic investigation of alcohol adsorption and oxidation on binary and ternary electrocatalysts in acid medium was performed in membraneless methanol fuel cell (MLMFC). The different nominal compositions of binary Pt–Sn/C, Pt–Rh/C and ternary Pt–Sn–Rh/C electrocatalysts were characterized by TEM, EDX, and XRD techniques. Energy dispersive X-ray spectroscopy and X-ray diffractometry confirmed the formation of Pt–Sn–Rh/C, Pt–Sn/C, Pt–Rh/C metal catalyst having typical Pt crystalline structure and the formation of Pt–Sn alloy. Electrochemical analyses obtained at room temperature by cyclic voltammetry and chronoamperometry showed that Pt–Sn–Rh/C (50:10:40) gives higher current density compared to that of Pt–Sn–Rh/C (50:40:10), Pt–Sn/C (50:50) and Pt–Rh/C (50:50). The power density obtained using Pt–Sn–Rh/C (50:10:40) (33.93 mW $cm^{-2}$) as anode catalyst in MLMFC was higher than that for Pt–Sn–Rh/C (50:40:10), Pt–Sn/C (50:50) and Pt–Rh/C (50:50) at room temperature, with catalyst loading of 2 mg $cm^{-2}$. In this work, carbon-supported binary Pt−Sn/C, Pt−Rh/C and ternary Pt−Sn−Rh/C anode catalysts were successfully tested in a single membraneless fuel cell using 1.0 M methanol as the fuel and 0.1 M sodium percarbonate as the oxidant in the presence of 0.5 M $H_2SO_4$ as the electrolyte at room temperature. Based on the experimental results, we conclude that the trimetallic combination of Pt–Sn–Rh/C (50:10:40) shows superior methanol electro-oxidation than bimetallic combinations of Pt–Sn/C (50:50) and Pt–Rh/C (50:50).
**Keywords :** Membraneless fuel cells; Platinum; Rhodium; Tin; Sodium percarbonate.

## 1. Introduction

Fuel cell is an eco-friendly power source, which converts chemical energy generated from a fuel and an oxidant into electrical energy, heat, and water by oxidoreduction reactions. A microfluidic fuel cell is defined as a device that incorporates all fundamental components of a fuel cell within a single microfluidic channel and its walls. Microfluidic fuel cells, which eliminate the proton exchange membrane and utilize the co-laminar flow nature of multistream in a microfluidic channel to separate the anolyte and catholyte, are considered as a promising alternative power source for portable devices [1, 2]. Microfluidic fuel cells eliminate the membrane-related problems, e.g. membrane degradation and water management, providing an opportunity to develop cost-effective and long-durable energy suppliers.

Methanol as a hydrogen-rich liquid for fuel cells is a very promising regarding its high power energy density, non toxicity, renewability and natural availability. Methanol is a attractive fuel as it can be produced in

great quantities form biomass and it is less toxic. In this context more active electrocatalysts are essential to enhance the methanol electro-oxidation [3]. Pure platinum is poisoned by strongly adsorbed species like CO, which is generated from the dissociation of organic molecules and thus the reactivity of platinum reduces. One of the ways to improve catalytic activity is to add co-catalyst with platinum, which results in adsorption of $OH_{ads}$ species at a lower potential. The $OH_{ads}$ species help to oxidize CO to $CO_2$ [4].

Platinum based bimetallic catalyst found to be most suitable anode electrocatalyst for the oxidation of alcohols [5]. The Pt based alloys such as Pt–Ru [6], Pt–Sn [7], Pt–Mo [8], Pt–Pd [9] Pt–Re [10], Pt–Ir [11], Pt–Ni [12] were reported as catalysts for methanol electro-oxidation. It has been reported that Pt–Sn catalyst shows the best catalytic performance for methanol electro-oxidation reaction (MOR) in the binary systems in acid media. This is explained by the role of Sn in water dissociation at lower potentials than Pt. The adsorbed surface OH groups on Sn sites react with the adsorbed CO on Pt sites to form $CO_2$. Consequently, making alloys with Sn is a convenient way to modify the electrocatalytic properties of Pt in order to overcome poisoning due to the methanol electro-oxidation intermediates, especially the adsorbed CO.

To further improve Pt electrocatalysts activity, Rh is introduced as a third metal in the Pt−Sn catalyst composition, which helps to enhance the dehydrogenation reaction and the C–C bond breakage during the oxidation of methanol. The main advantage of the introduction of this metal is the reduction of the oxidation potential of small organic molecules, coupled with the rise in current density. Souza et al. [13] studied the electro-oxidation of methanol on Pt, Rh and Pt–Rh electrodes. It was found that Rh was the less active electrocatalyst; on the other hand, the addition of small amounts of Rh to Pt increased to $CO_2$/acetaldehyde ratio. Thus, Pt–Rh/C electrocatalysts were considered promising candidates for methanol oxidation if a third element was added to improve the overall reaction rate. Recently, Kowal et al. [14] prepared a Pt–Rh–$SnO_2$/C electrocatalyst by depositing Pt and Rh atoms on carbon-supported $SnO_2$ nanoparticle and good results for methanol electro-oxidation were obtained. In the present study, we evaluated the catalytic activity for the methanol electro-oxidation reaction (MOR) by incorporating a third metal Rh to the Pt–Sn catalyst on a carbon support in membraneless methanol fuel cell (MLMFC). The performance of the Pt–Sn–Rh/C catalyst was compared with that of the Pt–Sn/C and Pt–Rh/C catalysts obtained by the co-impregnation reduction method.

## 2. Experimental

### 2.1. Material

The metal precursors used for the preparation of electrocatalysts were $H_2PtCl_6.6H_2O$ (from Merck), $SnCl_2.2H_2O$ (from Alfa Aesar), and $RhCl_3.3H_2O$ (from Merck). Vulcan XC-72R carbon black (from Cabot Corp.,) was used as a support for the catalysts. Graphite plates (3-cm long and 0.1-cm wide from E-TEK) were used as substrates for the catalyst to prepare the electrodes. Polytetrafluoroethylene (PTFE) (6%; Aldrich) dispersion was used to prepare the catalyst slurry. Iso-propanol and sodium borohydride (from Merck) was used as the solvent and reduction agent respectively. Methanol (from Merck), sodium percarbonate (from Riedel), and sulphuric acid (from Merck) were used as the fuel, oxidant, and electrolyte for electrochemical analysis, respectively. All the chemicals were of analytical grade. Pt/C (40-wt%; E-TEK) was used as the cathode catalyst.

### 2.2. Catalyst Preparation

Carbon-supported ternary Pt−Sn−Rh catalysts with different atomic ratios were synthesized by co-impregnation reduction method. The precursors were first suspended in iso-propanol and ultrasonicated for 3h. The carbon support Vulcan XC-72R, was preheated to 110°C for 2h and suspended in iso-propanol separately and ultrasonicated for 3 h. Precursor suspension is then added drop wise to carbon slurry [15]. The weight ratio of Pt−X/C (X = Sn, Rh, Sn−Rh) was controlled according to the targeted metal loading. Ultrasonic blending for 3h, of precursor and carbon suspension was carried out to ensure the proper impregnation of metal precursors on carbon support. The suspension was then kept at 70°C for 12 h to evaporate iso-propanol. To reduce metal precursors 0.2 M $NaBH_4$ solution was added to the mixture with stirring and further stirred for 3 h to confirm termination of reduction reaction. Finally the precipitate was collected by filtration, washed with deionized (DI) water, and dried at 70°C for 2 h. The electrocatalytic mixtures and the atomic ratios were $Pt_{100}$/C, $Pt_{50}Sn_{50}$/C, $Pt_{50}Rh_{50}$/C, $Pt_{50}Sn_{40}Rh_{10}$/C and $Pt_{50}Sn_{10}Rh_{40}$/C. The nominal loading of metals in the electrocatalysts was 40% wt. and the remaining was 60% wt. carbon.

### 2.3. Physical Characterization

The morphology, microstructure, and elemental composition of catalysts were investigated by transmission electron microscopy (TEM) and energy-dispersive X-ray (EDX) analysis under the Philips CM 120 microscope/EDX analyzer equipped with a $LaF_6$ filament. The particle size distribution and the mean particle size were also evaluated under TEM. The crystal structure of the synthesized electrocatalysts was characterized by powder X-ray diffraction (XRD) by using the Rigaku multiflex diffractometer (model RU-200 B) equipped with a Cu-$K_{\alpha 1}$ radiation source ($\lambda_{K\alpha 1}$ = 1.5406 $A^o$) operating at the room temperature. The tube current was 40 mA, with a tube voltage of 40 kV. The $2\theta$ angular regions between 20° and 90° were recorded at a scan rate of 5° $min^{-1}$. The mean particle size analyzed by TEM was verified by determining the crystallite size from the XRD pattern by using the Scherrer formula. Pt (2 2 0) diffraction peak was selected to calculate the crystallite size and lattice parameter of platinum.

According to the Scherrer's equation [16]

$$D = \frac{0.9\lambda_{K\alpha 1}}{\beta_{2\theta}\cos\theta_{max}} \qquad (1)$$

Where, $D$ is the average crystallite size, $\theta_{max}$ is the angle at the position of the peak maximum, $ß_{2\theta}$ is the width of the peak (in radians), 0.9 is the shape factor for spherical crystallite, and $\lambda_{K\alpha 1}$ is the wavelength of the X-rays used. The lattice parameters of the catalysts were estimated according to Equation 2 [16]:

$$a = \frac{\sqrt{2}\,\lambda_{K\alpha 1}}{\mathrm{Sin}\,\theta_{max}} \qquad (2)$$

Where, a is the lattice parameter (nm) and all other symbols have the same meanings as in Equation 1 [17].

### 2.4. Electrochemical Measurement

Electrochemical studies of the electrocatalysts were performed by using the thin porous coating technique [6, 12]. All electrochemical measurements were performed on an electrochemical workstation (model CHI6650; CH Instruments, USA) interfaced with a personal computer using the CHI software at the room temperature. A common three-electrode electrochemical cell based on the cyclic voltammetry (CV) and chronoamperometry (CA) techniques for the measurements. Catalyst-coated glassy carbon electrode (GCE; 3-mm diameter and 0.071 $cm^2$ of electrode area, CHI, USA) was used as the working electrode and platinum foil was used as the counter electrode. Ag/AgCl in saturated KCl was used as the reference electrode. The working electrode was prepared by applying the catalyst ink composed of 20 mg of the electrocatalysts in a solution of 50-mL water containing three drops of 6% PTFE suspension. The resulting mixture was treated in an ultrasound bath for 10 min to obtain a uniform dispersion. The catalyst slurry was then drop-cast on to a glassy carbon electrode and allowed to dry at 100°C for 30 min. For assessing the electrocatalytic activity of the working electrode, CV was obtained in 1.0 M methanol and 0.5 M $H_2SO_4$ solution with a scan rate of 50 mV $s^{-1}$. For the durability test, the chronoamperometric experiments were conducted at 0.1 V for 3000 s in the same electrolyte. Before each measurement, the solution was purged with high-purity nitrogen gas for at least 30 min to ensure oxygen-free measurements.

### 2.5. Single Cell Test

In the present study, we fabricated the membraneless methanol fuel cell (MLMFC) by using a laminar flow-based fuel cell configuration [18-21]. In this MLMFC, methanol was used as a fuel, sodium percarbonate as an oxidant, and $H_2SO_4$ as an electrolyte. Sodium percarbonate ($NaBO_3.4H_2O$) is a cheap, environment friendly, nontoxic, and large-scale industrial chemical, primarily used as a source of 'active oxygen' in detergents and as a mild antiseptic. In the crystalline state, sodium percarbonate existed as a dimeric peroxo-salt with water of hydration, but in the aqueous solution, it involved hydrogen peroxide [22], as shown in Eq. (3):

$$2Na_2CO_3.3H_2O_2 \rightarrow 2Na_2CO_3 + 3H_2O_2 \qquad (3)$$

In MLMFC, the aqueous fuel and oxidant streams flow in parallel in a single microchannel with the anode and cathode on the opposing sidewalls (Fig. 1). Graphite plates of 0.1-cm thickness served as the current collectors and catalyst support structures. The different anode and cathode catalysts were coated onto the graphite plates. For a single cell, the anode catalysts with different atomic ratios were prepared as follows: the catalyst ink was prepared by mixing the required quantity of catalyst with a solution of 50 mL water containing three drops of 6% PTFE dispersion in an ultrasonic bath for 10 min to obtain a uniform dispersion. The catalyst slurry was then spread onto the graphite plate by brushing, followed by drying at 100°C for 30 min to obtain the anode and cathode electrodes. The catalysts tested on the anode side were $Pt_{100}$/C, $Pt_{50}Sn_{50}$/C, $Pt_{50}Rh_{50}$/C, $Pt_{50}Sn_{40}Rh_{10}$/C and $Pt_{50}Sn_{10}Rh_{40}$/C with a catalyst loading 2 mg/cm$^2$. On the cathode side, $Pt_{100}$/C with catalyst loading 2 mg/cm$^2$ was used in all the experiments. The two catalyst-coated graphite plates were aligned to form a channel with 0.1 cm electrode-to-electrode distance (width), at 3-cm length, and 0.1-cm height. The anolyte (fuel and electrolyte) and catholyte (oxidant and electrolyte) streams flow in a laminar fashion over the anode and cathode, respectively. The electrode area along the microchannel wall between the inlets and the outlet (3-cm long and 0.1-cm wide) was used as the geometric surface area of the electrodes in this study (0.3 cm$^2$). The design has been described in detail elsewhere [23, 24]. The anolyte used in the anode side was 1.0 M methanol + 0.5 M $H_2SO_4$ and the catholyte used in the cathode side was 0.1 M percarbonate + 0.5 M $H_2SO_4$. The flow rate of each of the streams was 0.3 mL min$^{-1}$ (total flow rate of 0.6 mL min$^{-1}$). The MLMFC was operated at the room temperature. The current-voltage characteristics of MLMFC were measured on an electrochemical workstation and the data was verified by using a multi-meter (MASTECH® MAS830L).

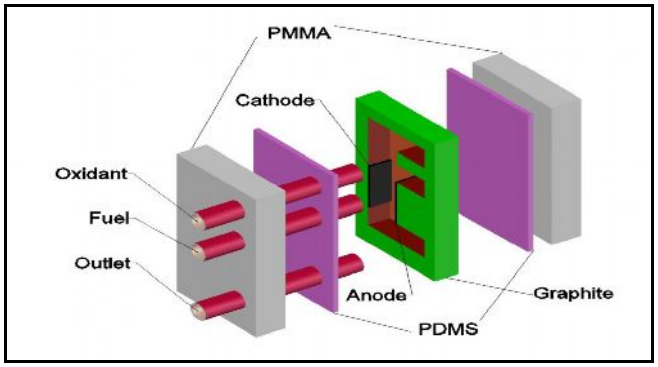


**Fig. 1. Schematic of the E-shaped membraneless laminar flow-based fuel cell with graphite plates molded with poly(dimethylsiloxane) (PDMS) and sealed with poly(methylmethacrylate) (PMMA).**

## 3. Results and Discussions

### 3.1. Physical Characterization

#### 3.1.1. X-Ray Diffraction

X-Ray Diffraction (XRD) patterns of $Pt_{100}$/C, $Pt_{50}Sn_{50}$/C, $Pt_{50}Rh_{50}$/C, $Pt_{50}Sn_{40}Rh_{10}$/C and $Pt_{50}Sn_{10}Rh_{40}$/C catalysts are shown in Fig. 2. The peak at 25–30° observed in all diffraction patterns of the carbon-supported catalysts is attributed to the (0 0 2) plane of the hexagonal structure of the Vulcan XC-72R carbon support [11]. The diffraction peaks at around 40°, 47°, 67°, and 82° are attributed to the Pt (1 1 1), (2 0 0), (2 2 0), and (3 1 1) crystalline planes, respectively, which represents the typical character of crystalline Pt with face-centered cubic (FCC) crystalline structure. These diffraction peaks are shifted to lower 2$\theta$ values in the Sn-containing catalysts with respect to the corresponding peaks in the pure Pt catalyst. The shift of the Pt-peaks to the lower angles reveals alloy formation between the angle Pt and Sn, which is caused by the incorporation of Sn in the fcc structure of Pt [25]. In the case of $Pt_{50}Rh_{50}$/C, the addition of Rh to Pt promoted a shift in the Pt-peaks to higher 2θ values, indicating the formation of an alloy upon incorporation of Rh into the platinum structure [26]. The $SnO_2$ (2 1 1) peaks are visible in the XRD patterns of Sn-containing catalysts. No peaks of metallic Rh or Rh oxides were detected in the Pt–Sn–Rh catalysts, but their presence cannot be discarded because they may be present in a very small particle size or even in an amorphous form. The lattice parameters and the average crystallite size of the catalysts obtained from the XRD patterns are listed under Table 1.

**Table 1 Characterization parameters for the $Pt_{100}$/C, $Pt_{50}Sn_{50}$/C, $Pt_{50}Rh_{50}$/C, $Pt_{50}Sn_{40}Rh_{10}$/C and $Pt_{50}Sn_{10}Rh_{40}$/C catalysts.**

| Electrocatalysts | | (2 2 0) Diffraction peak position (2θ°) | Lattice parameter (Å) | Average crystallite size from XRD (nm) | Average Particle size from TEM (nm) |
|---|---|---|---|---|---|
| Nominal | Experimental | | | | |
| $Pt_{100}$/C | $Pt_{100}$/C | 67.68 | 0.3912 | 2.8 | - |
| $Pt_{50}Sn_{50}$/C | $Pt_{53}Sn_{47}$/C | 66.6 | 0.3968 | 4.1 | 4.0 |
| $Pt_{50}Rh_{50}$/C | $Pt_{51}Rh_{49}$/C | 68.3 | 0.3881 | 2.5 | 2.4 |
| $Pt_{50}Sn_{40}Rh_{10}$/C | $Pt_{51}Sn_{38}Rh_{11}$/C | 66.74 | 0.3961 | 3.3 | 3.0 |
| $Pt_{50}Sn_{10}Rh_{40}$/C | $Pt_{49}Sn_9Rh_{42}$/C | 67.08 | 0.3943 | 2.7 | 2.3 |

The fcc lattice parameters were evaluated from the angular position of the (2 2 0) peaks and the calculated value for Pt−Rh/C electrocatalyst (0.3881 nm) was lower than that of Pt/C electrocatalyst (0.3912 nm), indicating a lattice contraction caused by the incorporation of Rh into the fcc structure of platinum after alloying. For Pt−Sn/C electrocatalyst the fcc lattice parameter measured (0.3968 nm) was larger than the one obtained for Pt/C electrocatalyst, due to a lattice expansion after alloying, indicating that part of Sn was incorporated in the fcc structure of Pt. The lattice parameters of the ternary catalysts were larger than that of Pt–Rh/C and smaller than that of Pt–Sn/C. The lattice parameters of the ternary catalysts were larger than that of Pt–Rh/C and smaller than that of Pt–Sn/C. This intermediate value of the lattice parameter of the ternary catalysts can be explained in two ways: (1) a lower amount of Sn alloyed with Pt. Indeed, as observed in other ternary catalysts, the presence of a third non-alloyed metal can cause a decrease of the degree of alloying of the binary base alloy with respect to the binary catalyst [27, 28]. (2) The formation of a ternary alloy. In view of the fact that Rh alloys with Pt, the formation of a ternary Pt–Sn–Rh alloy is likely. To support this hypothesis, it was found that the lattice parameter of the Pt-alloy linearly decreases with increasing the nominal Rh content in the catalyst, as shown in Fig. 3. The average particle size was estimated using the Scherrer equation (Table 1). The particle sizes for Pt−Rh/C, Pt−Sn/C, and Pt−Sn−Rh/C electrocatalysts were in the range of ~2.5–4.1 nm.

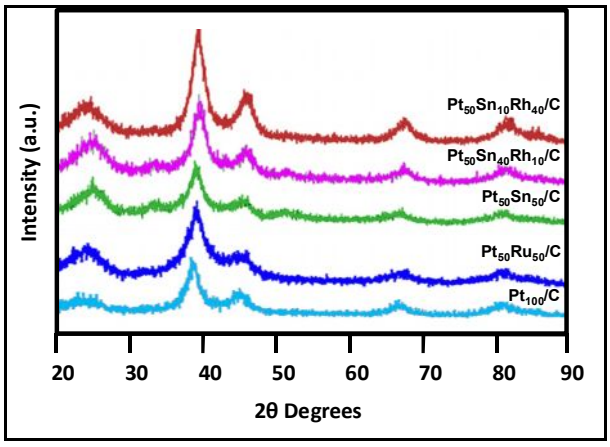


**Fig. 2. X-Ray diffraction patterns of $Pt_{100}$/C, $Pt_{50}Sn_{50}$/C, $Pt_{50}Rh_{50}$/C, $Pt_{50}Sn_{40}Rh_{10}$/C and $Pt_{50}Sn_{10}Rh_{40}$/C catalysts.**

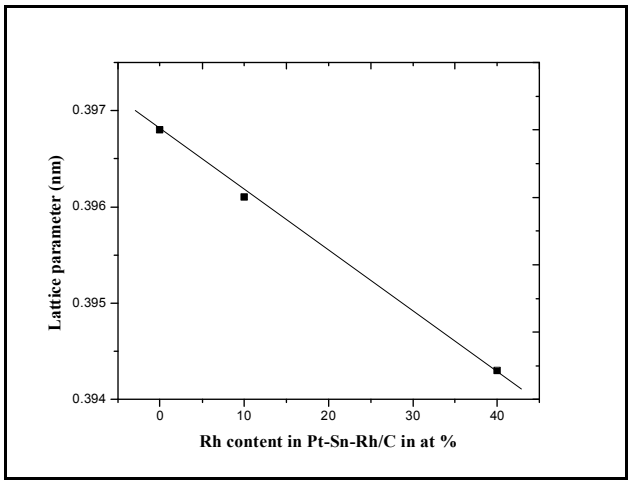


**Fig. 3. Dependance of the FCC lattice parameter of the Pt–Sn–Rh/C alloy catalyst on Rh content.**

### 3.1.2. Transmission Electron Microscopy (TEM)

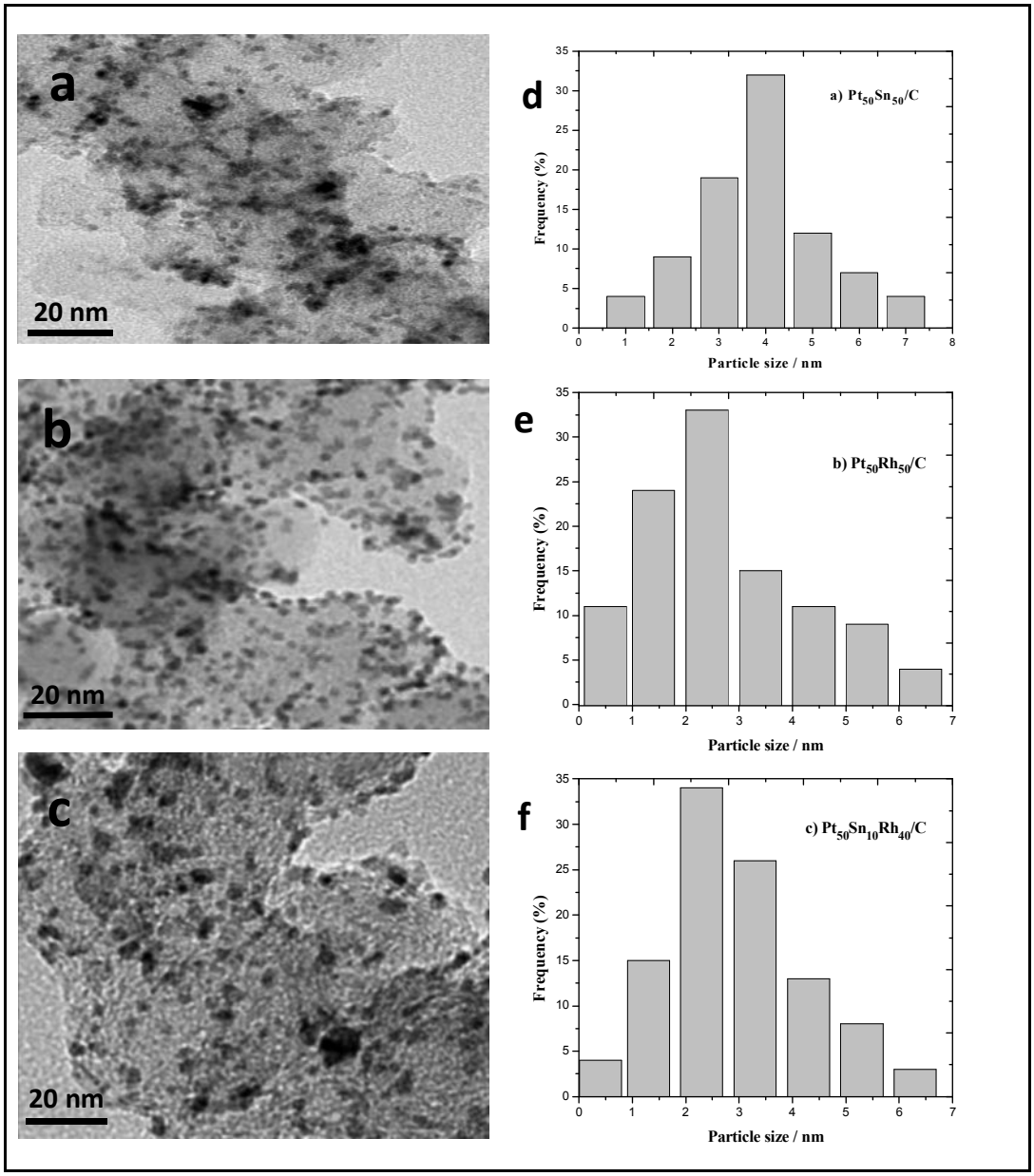


**Fig. 4. TEM images and histograms of a and d) $Pt_{50}Sn_{50}$/C, b and e) $Pt_{50}Rh_{50}$/C and c and f) $Pt_{50}Sn_{10}Rh_{40}$/C catalysts.**

TEM images and histograms of the $Pt_{50}Sn_{50}$/C, $Pt_{50}Rh_{50}$/C, and $Pt_{50}Sn_{10}Rh_{40}$/C catalysts are shown in Fig. 4. The micrographs of the electrocatalysts showed that all the catalysts had a good dispersion on the Vulcan XC-72R with a size in the same range and following a log-normal size distribution [29-31]. The average particle size for $Pt_{50}Sn_{50}$/C, $Pt_{50}Rh_{50}$/C, and $Pt_{50}Sn_{10}Rh_{40}$/C catalysts was 2–4 nm. In comparison to $Pt_{50}Sn_{50}$/C, and $Pt_{50}Rh_{50}$/C, the mean particle size of $Pt_{50}Sn_{10}Rh_{40}$/C was smaller. The variation in the mean particle size for these catalysts was quite similar in both the cases (TEM and XRD), indicating a good particle dispersion without formation of large particle aggregates (Table 1).

### 3.1.3. Energy Dispersive X-ray (EDX) Analysis

EDX analyses of all the $Pt_{50}Sn_{50}$/C, $Pt_{50}Rh_{50}$/C and $Pt_{50}Sn_{10}Rh_{40}$/C catalysts are shown in Fig. 5. Fig. 5a–c indicates the presence of Pt, Sn, and C; Pt, Rh, and C; and both the combinations of Pt, Sn, Rh, and C, respectively. The EDX results are shown in Table 1. The prepared catalysts had the desired elements with some variation in their composition. The EDX results of the binary Pt–Sn/C and Pt–Rh/C and the ternary Pt–Sn–Rh/C catalysts were extremely close to the nominal values, indicating that the metals were loaded onto the carbon support without any obvious loss.

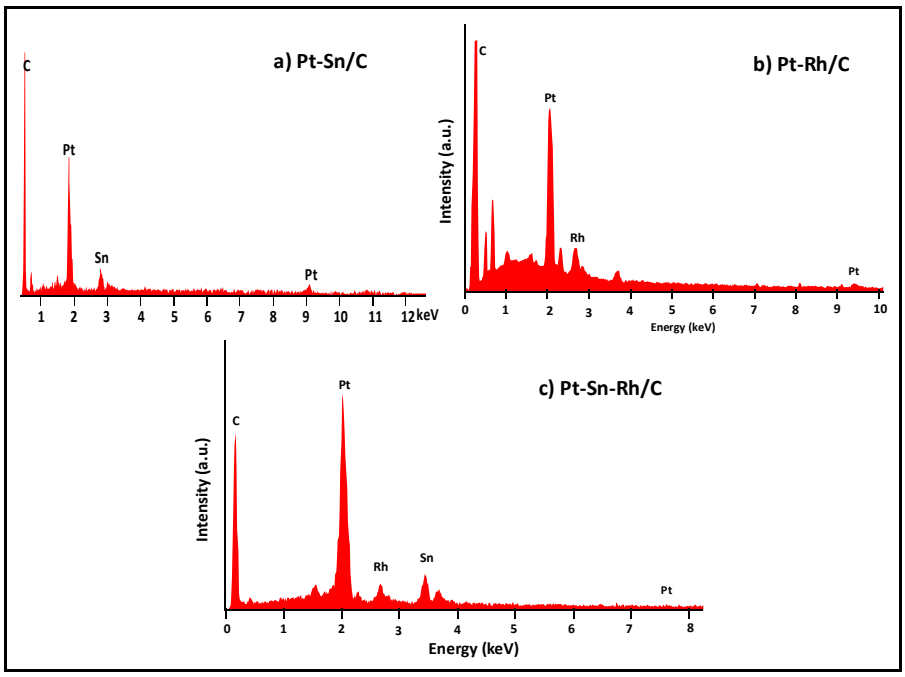


**Fig. 5. EDX spectra of a) $Pt_{50}Sn_{50}$/C, b) $Pt_{50}Rh_{50}$/C and c) $Pt_{50}Sn_{10}Rh_{40}$/C catalysts.**

## 3.2. Electrochemical Characterization

### 3.2.1. Cyclic Voltammetry

Fig. 6a shows the cyclic voltammograms (CV) of the $Pt_{100}$/C, $Pt_{50}Sn_{50}$/C, $Pt_{50}Rh_{50}$/C, $Pt_{50}Sn_{40}Rh_{10}$/C and $Pt_{50}Sn_{10}Rh_{40}$/C electrocatalysts, obtained in 0.5 mol $dm^{-3}$ $H_2SO_4$, at a scan rate of 50 mV $s^{-1}$ between 0.05 and 0.8 V (*vs.* Ag/AgCl) in the absence of methanol and at room temperature. For the five electrocatalysts compositions presented herein, the area of adsorption/desorption of hydrogen at the platinum surface for E < 0.4 V *vs.* Ag/AgCl can be clearly seen. This region is distorted as compared to pure Pt and this is associated with the presence of transition metals such as ruthenium, iridium, osmium, etc. [25]. Beyond this potential value, one observes the formation of layers of oxides and hydroxides due to the activation of interfacial water molecules by the presence of tin and rhodium. The presence of transition metals leads to a larger double layer region in these catalysts, which has been observed before [32, 33].

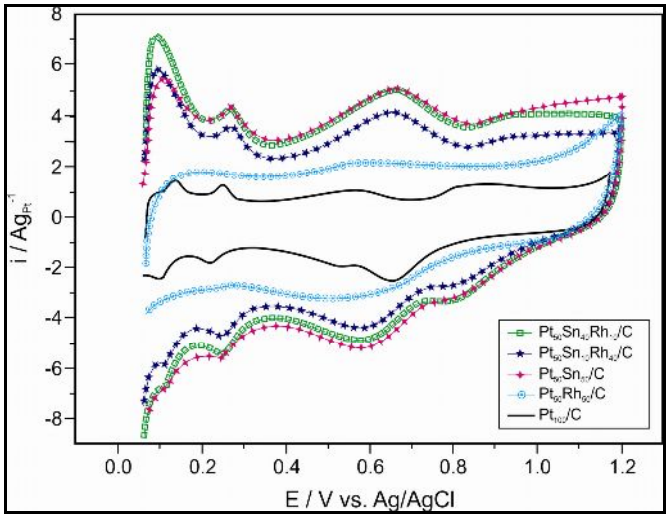


**Fig. 6a. Cyclic voltammetry of $Pt_{100}$/C, $Pt_{50}Sn_{50}$/C, $Pt_{50}Rh_{50}$/C, $Pt_{50}Sn_{40}Rh_{10}$/C and $Pt_{50}Sn_{10}Rh_{40}$/C electrocatalysts in 0.5 M $H_2SO_4$ at room temperature with a scan rate of 50 mV/s.**

Fig. 6b shows the cyclic voltammograms of methanol oxidation under acidic conditions (1.0 M $CH_3OH$ and 0.5 M $H_2SO_4$) catalyzed by $Pt_{100}$/C, $Pt_{50}Sn_{50}$/C, $Pt_{50}Rh_{50}$/C, $Pt_{50}Sn_{40}Rh_{10}$/C and $Pt_{50}Sn_{10}Rh_{40}$/C catalysts. All of the current values were normalized by the geometric surface area of the electrode used. The CV curves (Fig. 6b) depict the presence of a peak in the potential range of the positive sweep and another peak in the negative sweep. The peak in the positive sweep is associated with the methanol oxidation, and the peak in the negative sweep is related to the oxidation of carbonaceous intermediate products from incomplete methanol oxidation. Table 2 summarizes the CV results of $Pt_{100}$/C, $Pt_{50}Sn_{50}$/C, $Pt_{50}Rh_{50}$/C, $Pt_{50}Sn_{40}Rh_{10}$/C and $Pt_{50}Sn_{10}Rh_{40}$/C electrocatalysts including the positive peak potentials and the corresponding peak current densities of MOR.

**Table 2 CV results of $Pt_{100}$/C, $Pt_{50}Sn_{50}$/C, $Pt_{50}Rh_{50}$/C, $Pt_{50}Sn_{40}Rh_{10}$/C and $Pt_{50}Sn_{10}Rh_{40}$/C electrocatalysts at room temperature.**

| Catalyst | Scan rate 50 mV/s | |
|---|---|---|
| | Positive peak potential (V vs. Ag/AgCl) | Peak current density (mA/cm$^2$) |
| **$Pt_{100}$/C** | 0.92 | 9.91 |
| **$Pt_{50}Rh_{50}$/C** | 0.97 | 15.53 |
| **$Pt_{50}Sn_{50}$/C** | 0.96 | 17.60 |
| **$Pt_{50}Sn_{40}Rh_{10}$/C** | 0.95 | 22.31 |
| **$Pt_{50}Sn_{10}Rh_{40}$/C** | 0.92 | 25.95 |

The CV results show that pure $Pt_{100}$/C catalysts (Fig. 6b) do not behave as an appropriate anode for MOR due to its poisoning by strongly adsorbed intermediates such as CO. However, the introduction of Sn and Rh promotes the electrocatalytic activity. The MOR starts at approximately 0.4 V on the $Pt_{50}Sn_{50}$/C electrode, while the onset potential on $Pt_{50}Rh_{50}$/C was noted at 0.4 V vs. Ag/AgCl. This observation can be explained by the more pronounced oxophilic character of tin at low potentials in comparison with rhodium [26, 33-34]. Furthermore, the presence of both co-catalysts, Rh and Sn, significantly reduced the onset potential to approximately 0.3 V vs. Ag/AgCl and raised the current density at the $Pt_{50}Sn_{40}Rh_{10}$/C and $Pt_{50}Sn_{10}Rh_{40}$/C electrocatalyst. The superior activity of the $Pt_{50}Sn_{10}Rh_{40}$/C electrocatalyst can be attributed to the modification of electronic properties of platinum and to the presence of oxide species resulting in a combination of electronic effect and bifunctional mechanism, as well assumed for various Pt-based electrocatalysts [35-37]. The first electro-oxidation peak of methanol on $Pt_{50}Sn_{50}$/C is at 0.96 V (vs. Ag/AgCl), which is 30 mV higher than that of $Pt_{50}Sn_{10}Rh_{40}$/C. The current density at the first peak of methanol electro-oxidation on $Pt_{50}Sn_{10}Rh_{40}$/C is 25.95 mA/cm$^2$ is which is higher than that on $Pt_{50}Sn_{50}$/C with a difference of 8.35 mA/cm$^2$, but less than that of $Pt_{50}Sn_{40}Rh_{10}$/C. Again, the ternary compositions ($Pt_{50}Sn_{10}Rh_{40}$/C) presented much higher current densities than the binary catalysts, indicating that the activity of the ternary electrocatalysts toward MOR was much better than that of the binary compositions.

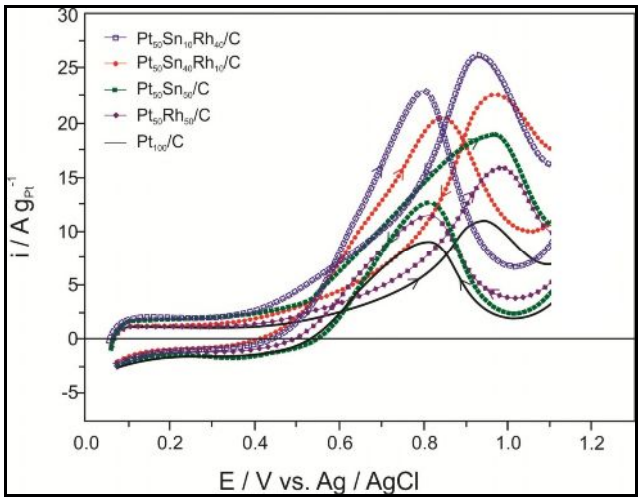


**Fig. 6b. Cyclic voltammetry of $Pt_{100}$/C, $Pt_{50}Sn_{50}$/C, $Pt_{50}Rh_{50}$/C, $Pt_{50}Sn_{40}Rh_{10}$/C and $Pt_{50}Sn_{10}Rh_{40}$/C electrocatalysts in 0.5 M $H_2SO_4$ and 1.0 M methanol at room temperature at a scan rate of 50 mV/s.**

### 3.2.2. Chronoamperometry (CA)

The $Pt_{100}$/C, $Pt_{50}Sn_{50}$/C, $Pt_{50}Rh_{50}$/C, $Pt_{50}Sn_{40}Rh_{10}$/C and $Pt_{50}Sn_{10}Rh_{40}$/C electrocatalyst performances for methanol oxidation were studied by chronoamperometry (CA) at 0.4 V *vs* Ag/AgCl for 1000 s to evaluate both the electrocatalytic activity of the catalysts and the poisoning of the active surface under continuous operation conditions. Fig. 7 shows the representative chronoamperograms obtained for the different electrocatalysts whose current densities were normalized by Pt mass. During the first 5 min, a sharp decrease in the current density. Followed by relative stabilization was noted. This occurs because the active sites were initially free from the adsorbed/oxidized methanol molecules. However, as the reaction proceeds, the adsorption rate of a new methanol molecule depends on the availability of the catalyst active site. This reaction is metal-dependent and proceeds faster (high current density) in the case of metals with a good ability to oxidize the intermediate species responsible for poisoning of the catalytic sites (CO, $CH_x$, $CH_3CHO$, and $CH_3COOH$) [32]. Thus, the surface becomes unstable, and the phenomena such as crystallization, segregation of the metal surface, and agglomeration of particles may occur to create new catalytic sites. The latter are quickly poisoned, thereby contributing to the continuous decrease in the current [16]. The compositions $Pt_{100}$/C, $Pt_{50}Sn_{50}$/C, $Pt_{50}Rh_{50}$/C, $Pt_{50}Sn_{40}Rh_{10}$/C and $Pt_{50}Sn_{10}Rh_{40}$/C gave rise to extremely rapid rates of poisoning of the catalytic sites, resulting in a very low activity. However, ternary material ($Pt_{50}Sn_{10}Rh_{40}$/C) had a good ability to overcome catalyst poisoning, thus furnishing a high current density [26].

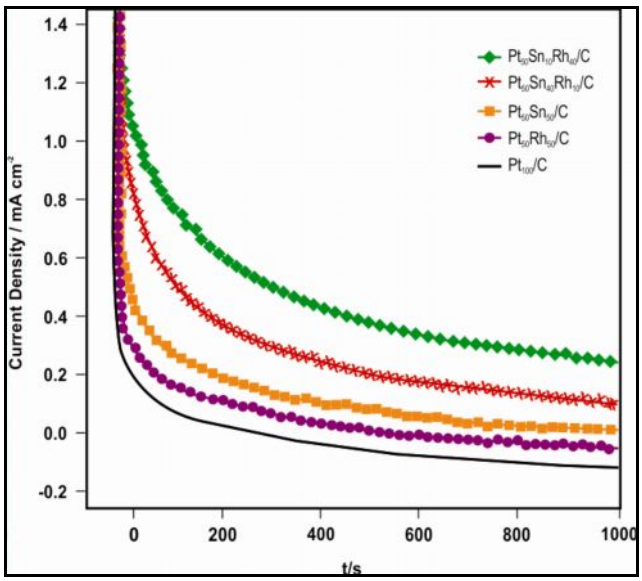


**Fig. 7. Chronoamperometry of $Pt_{100}$/C, $Pt_{50}Sn_{50}$/C, $Pt_{50}Rh_{50}$/C, $Pt_{50}Sn_{40}Rh_{10}$/C and $Pt_{50}Sn_{10}Rh_{40}$/C electrocatalysts at the room temperature.**

The ternary $Pt_{50}Sn_{10}Rh_{40}/C$ and $Pt_{50}Sn_{40}Rh_{10}/C$ electrocatalysts demonstrated higher current than the binary $Pt_{50}Sn_{50}/C$ and $Pt_{50}Rh_{50}/C$ electrocatalysts. Higher current obtained for the ternary electrocatalysts may be explained by the operation of a beneficial synergistic effect between Sn and Rh, which may indicate an increase in the structural defects or roughness, making the ternary electrocatalysts better candidates for MOR. Furthermore, the addition of Rh to the Pt–Sn alloy electrocatalysts can lead to an increase in the surface oxophilic character, thus increasing the Sn–O bond strength and the acidity of the Sn–OH sites, favoring the bifunctional character of MOR [26]. The beneficial effect of Rh addition has been reported earlier for Pt–Sn/C and Pt–Ru/C catalysts. Indeed, significant improvements in methanol and methanol oxidation were observed [26, 33-34]. These observations suggest that the performance of Pt–Sn–Rh/C electrocatalysts depends greatly on its atomic ratios and its preparation.

### 3.3. Single Cell Performance

The $Pt_{100}/C$, $Pt_{50}Sn_{50}/C$, $Pt_{50}Rh_{50}/C$, $Pt_{50}Sn_{40}Rh_{10}/C$ and $Pt_{50}Sn_{10}Rh_{40}/C$ catalysts were evaluated as anode catalysts for MOR by single MLMFC. The polarization and power density curves of different catalyst are presented in Fig. 8. When $Pt_{100}/C$ was used as the anode catalyst, the performance of MLMFC was found to be poor. The open-circuit potential (OCP) of $Pt_{100}/C$ was 0.52 V, which is far less than that of the reversible OCP (1.145 V) [38], which can be attributed mainly to the poor catalytic activity toward MOR. The results of MLMFC adopting to different catalysts are summarized in Table 3. When the current was normalized to the geometric area of a single cell, it was observed that the cell performance of the $Pt_{50}Sn_{10}Rh_{40}/C$ catalyst was better than that of other catalysts. In the low-current discharging region, the power drawn from a single cell was almost the same for all catalysts, except for $Pt_{50}Rh_{50}/C$, and $Pt_{100}/C$. However, as the voltage reached approximately 0.3 V, $Pt_{50}Sn_{10}Rh_{40}/C$ started drawing more current compared to others. The OCP for $Pt_{50}Sn_{50}/C$ catalyst was 0.63 V lower than that for $Pt_{50}Sn_{10}Rh_{40}/C$ (0.71 V). In addition, a rapid initial fall in the cell voltage was noted for all catalysts, which was due to the slow initial MOR reaction at the electrode surface. After an initial drop of 0.5 V, the change in the slope of the polarization curve for $Pt_{50}Sn_{10}Rh_{40}/C$, and it started drawing more current. This event can be attributed to the more effective catalytic ability of $Pt_{50}Sn_{10}Rh_{40}/C$, once the MOR reaction is initiated. Based on the peak power density drawn from a single cell, $Pt_{50}Sn_{10}Rh_{40}/C$ is the best anode catalyst with a peak power density value of 33.93 $mW/cm^2$.

**Table 3 Summary of the performance of single fuel cell tests using 2 mg $cm^{-2}$ catalyst loading, 40 wt% catalyst on carbon)**

| Anode Catalysts | Open circuit voltage (V) | Maximum power density ($mW/cm^2$) | Maximum Current density ($mA/cm^2$) |
|---|---|---|---|
| **$Pt_{100}/C$** | **0.52** | **4.47** | **43.67** |
| **$Pt_{50}Rh_{50}/C$** | **0.55** | **16.37** | **110.33** |
| **$Pt_{50}Sn_{50}/C$** | **0.63** | **22.91** | **159.51** |
| **$Pt_{50}Sn_{40}Rh_{10}/C$** | **0.65** | **30.33** | **192.74** |
| **$Pt_{50}Sn_{10}Rh_{40}/C$** | **0.71** | **33.93** | **224.23** |

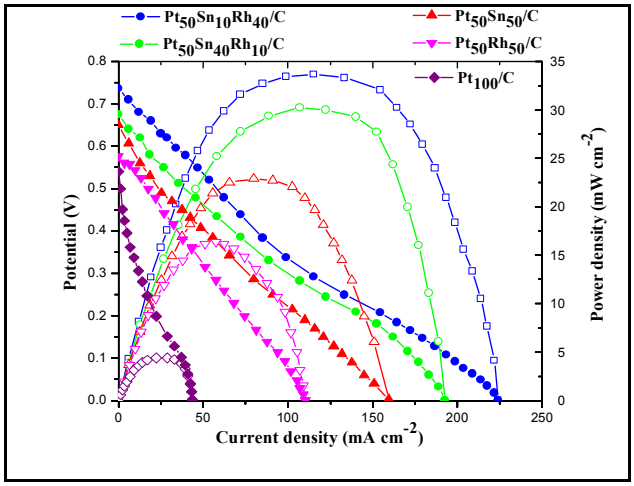


**Fig. 8. Polarization and power density curves of different catalyst at 2 mg $cm^{-2}$ catalyst loading on the anode and cathode at the room temperature.**

The addition of Sn clearly enhanced the MOR reaction as observed from the polarization curves that the electrocatalysts containing Sn showed higher open circuit voltage (OCV). $Pt_{50}Sn_{50}/C$, $Pt_{50}Sn_{40}Rh_{10}/C$ and $Pt_{50}Sn_{10}Rh_{40}/C$ showed OCV of 0.63 V, 0.65 V and 0.71 V, respectively, in comparison to $Pt_{50}Rh_{50}/C$ and $Pt_{100}/C$, which showed OCV of 0.55 V and 0.52 V, respectively. The comparison of both the bimetallic catalysts showed a peak power density of $Pt_{50}Sn_{50}/C$ (22.91 $mW/cm^2$), which was higher than that of $Pt_{50}Rh_{50}/C$ (16.37 $mW/cm^2$).

The catalytic activity was attributed to the synergy between the three constituents of the electrocatalyst, where $SnO_2$ strongly adsorbs water and precludes the Pt and Rh sites from reacting with $H_2O$ to M−OH, making Pt and Rh sites available for methanol oxidation. It is concluded that the $SnO_2$ reacts with $H_2O$ and provides OH species to oxidize the dissociated CO at Rh sites, while Pt facilitates methanol dehydrogenation. Thus, the good activity for methanol oxidation of the Pt−Sn−Rh/C electrocatalysts increases the cell performance. It can be observed that, for $Pt_{50}Rh_{50}/C$, $Pt_{50}Sn_{40}Rh_{10}/C$ and $Pt_{50}Sn_{10}Rh_{40}/C$ combination containing 50, 10 and 40 atomic ratios of Rh, the peak power densities were 16.37, 30.33 and 33.93 $mW/cm^2$, respectively. This observation indicates that the presence of only a small amount of Sn in the Pt−Sn−Rh/C catalyst aids in the MOR. Even under working conditions of the fuel cells, the best performance is achieved with lower Sn atomic ratios (near 10 wt%). Similar results were observed by Ribeiro et al. [25] for methanol oxidation by using catalysts prepared by the Pechini–Adams modified method.

## 4. Conclusions

In this study, we observed that the co-impregnation reduction process could be effectively used for the preparation of $Pt_{100}/C$, $Pt_{50}Sn_{50}/C$, $Pt_{50}Rh_{50}/C$, $Pt_{50}Sn_{40}Rh_{10}/C$ and $Pt_{50}Sn_{10}Rh_{40}/C$ eletrocatalysts for methanol oxidation in $H_2SO_4$ solution. The X-ray diffractograms of the electrocatalysts showed the typical fcc structure of platinum and platinum alloys with the presence of the cassiterite $SnO_2$ phase. The addition of Rh to Pt promotes a small decrease in the lattice parameter of the Pt structure (0.3881 nm), whereas the addition of Sn increases this value (0.3968 nm). TEM measurements revealed a decrease in the mean particle size of the catalysts for the ternary compositions, because the structural change was beneficial for the catalytic activity of the compositions. EDX analysis indicated that the experimental composition is in agreement with the nominal composition of the catalyst, which confirms the formation of $Pt_{50}Sn_{50}/C$, $Pt_{50}Rh_{50}/C$, and $Pt_{50}Sn_{10}Rh_{40}/C$ metal catalysts with the typical Pt crystalline structure and the formation of Pt−Sn alloy. CV results showed that $Pt_{50}Sn_{10}Rh_{40}/C$ is more active in MOR than in other catalysts. The onset potential for this reaction was found to be 0.2 V vs. Ag/AgCl, which suggests that the activation occurs at the electrode surface by a ligand effect. CA results showed that the ternary $Pt_{50}Sn_{40}Rh_{10}/C$ and $Pt_{50}Sn_{10}Rh_{40}/C$ catalysts gave higher current than the binary $Pt_{50}Sn_{50}/C$ and $Pt_{50}Rh_{50}/C$ catalysts at a steady condition. The enhanced methanol oxidation activity by the ternary $Pt_{50}Sn_{10}Rh_{40}/C$ catalyst was mainly ascribed to the synergistic effect between Sn and Rh and to the smaller particle size. In this study, for the first-time, carbon-supported binary $Pt_{50}Sn_{50}/C$, $Pt_{50}Rh_{50}/C$, and ternary $Pt_{50}Sn_{40}Rh_{10}/C$ and $Pt_{50}Sn_{10}Rh_{40}/C$ anode catalysts were successfully tested in a single membraneless fuel cell using 1.0 M methanol as fuel and 0.1 M sodium percarbonate as the oxidant in the presence of 0.5 M $H_2SO_4$ as the electrolyte. Based on the peak power density drawn from a single cell, $Pt_{50}Sn_{10}Rh_{40}/C$ was found to be the best anode catalyst with a peak power density of 33.93 $mW/cm^2$ among the tested catalysts. Further work is necessary to characterize the catalysts by using different surface analysis techniques and to conduct tests of these electrocatalysts in microfluidic membraneless fuel cells.

## References

1. Kjeang E, Djilali N and Sinton D., Microfluidics fuel cells: A review, J Power Sources 2009;186:353-369.
2. Shaegh SAM, Nguyen NT and Chan SH. A review on membraneless laminar flow-based fuel cells, Int. J Hydrogen Energy 2011;36:5675-5694.
3. Lamy C, Lima A, LeRhun V, Delime F, Coutanceau C and Le´ger J-M, Recent advances in the development of direct alcohol fuel cells. J Power Sources 2002;105:283-296.
4. Wang ZB, Yin GP, Zhang J, Sun YC, Shi PF and Wang ZB. Investigation of ethanol electro-oxidation on a Pt-Ru-Ni/C catalyst for a direct ethanol fuel cell, J Power Sources 2006;160:37-43.
5. Gupta SS, Mahapatra SS and Datta J. A potential anode material for the direct alcohol fuel cell, J Power Sources 2004;131:169-174.

6. Neto AO, Dias RR, Tusi MM, Linardi M and Spinac´e EV. Electro-oxidation of methanol and ethanol using PtRu/C, PtSn/C and PtSnRu/C electrocatalysts prepared by an alcohol-reduction process, J. Power Sources 2007;166:87–91.
7. Colmati F, Antolini E and Gonzalez ER. Ethanol oxidation on a carbon-supported $Pt_{75}Sn_{25}$ electrocatalyst prepared by reduction with formic acid: Effect of thermal treatment, Appl. Catal B 2007;73:106-115.
8. Lee E, Murthy A and Manthiram A. Effect of Mo addition on the electrocatalytic activity of Pt-Sn-Mo/C for direct ethanol fuel cells. Electrochimica Acta 2001;56:1611-1618.
9. Lopes T, Antolini E and Gonzalez ER. Carbon supported Pt-Pd alloy as an ethanol tolerant oxygen reduction electrocatalyst for direct ethanol fuel cells. Int J Hydrogen Energy 2008;33:5563-5570.
10. Tayal J, Rawat B and Basu S. Effect of addition of rhenium to Pt-based anode catalysts in electro-oxidation of ethanol in direct ethanol PEM fuel cell. International Journal of Hydrogen energy 2012;37:4597-4605.
11. Tayal J, Rawat B and Basu S. Bi-metallic and tri-metallic Pt-Sn/C, Pt-Ir/C, Pt-Ir-Sn/C catalysts for electro-oxidation of ethanol in direct ethanol fuel cell. International Journal of Hydrogen energy 2011;36:14884-14897.
12. Spinace EV, Linardi M and Neto AO. Co-catalytic effect of nickel in the electro-oxidation ofmethanol on binary Pt–Sn electrocatalysts. Electrochemistry Communications 2005;7:365–369.
13. de Souza JPI, Queiroz SL, Bergamaski K, Gonzalez ER and Nart FC. Electro-oxidation of ethanol on Pt, Rh, and PtRh electrodes. A study using DEMS and in-situ FTIR techniques. J Phys Chem B 2002;106:9825-9830.
14. Kowal A, Li M, Shao M, Sasaki K, Vukmirovic MB, Zhang J, Marinkovic NS, Liu P, Frenkel AI and Adzic RR. Ternary $Pt/Rh/SnO_2$ electrocatalysts for oxidizing ethanol to $CO_2$. Nat Mat 2009;8:325-330.
15. Yang B, Lu Q, Wang Y, Zhuang L, Lu J and Liu P. Simple and low-cost preparation method for highly dispersed PtRu/C catalysts. Chem Mater 2003;15:3552-3557.
16. Radmilovic V, Gasteiger HA and Ross Jr. PN. Structure and chemical composition of a supported Pt-Ru electrocatalyst for methanol oxidation. J Catal 1995;154:98–106.
17. Beyhan S, Leger J-M and Kadırgan F. Pronounced synergetic effect of the nano-sized PtSnNi/C catalyst form ethanol oxidation in direct ethanol fuel cell. Applied Catalysis B: Environmental 2013;130–131:305–313.
18. Arun A, Gowdhamamoorthi M, Ponmani K, Kiruthika S and Muthukumaran B. Electrochemical characterization of Pt-Ru-Ni/C anode electrocatalyst for methanol electrooxidation in membraneless fuel cells, RSC Advances 2015;5:49643-49650.
19. Gowdhamamoorthi M, Arun A, Kiruthika S and Muthukumaran B. percarbonate as novel fuel for enhanced performance of membraneless fuel cells. Ionics 2014;20:1723-1728.
20. Arun A, Gowdhamamoorthi M, Kiruthika S and Muthukumaran B. Analysis of membraneless methanol fuel cell using percarbonate as an oxidant. J of The Electrochemical Society 2013;161:F1-F7.
21. Ponmani K, Durga S, Gowdhamamoorthi M, Kiruthika S and Muthukumaran B. Influence of fuel and media on membraneless sodium percarbonate fuel cell. Ionics 2014;20:1579-1589.
22. Cotton FA, Wilkinson G. Advanced inorganic chemistry. New York: Wiley Interscience; 1988.
23. Choban ER, Markoski LJ, Wieckowski A and Kenis PJA. Microfluidic fuel cell based on laminar flow. J Power Sources 2004;128:54-60.
24. Jayashree RS, Yoon SK, Brushett FR, Lopez-Montesinos PO, Natarajan D, Markoski LJ and Kenis PJA. On the performance of membraneless laminar flow-based fuel cells. J Power Sources 2010;195:3569–3578.
25. Ribeiro J, dos Anjos DM, Kokoh KB, Coutanceau C, L´eger J-M, Olivi P, de Andrade AR and Tremiliosi-Filho G. Carbon-supported ternary PtSnIr catalysts for direct ethanol fuel cell. Electrochim Acta 2007;52:6997–7006.
26. Spinace EV, Dias RR, Brandalise M, Linardi M and Neto AO. Electro-oxidation of ethanol using PtSnRh/C electrocatalysts prepared by an alcohol-reduction process. Ionics 2010;16:91-95.
27. Venkataraman R, Kunz HR and Fenton JM. Development of New CO Tolerant Ternary Anode catalysts for proton exchange membrane fuel cells. J Electrochem Soc 2003;150:A278-A284.
28. Jusys Z, Schmidt TJ, Dubau L, Lasch K, Jorissen L, Garche J and Behm RJ. Activity fo $PtRuMeO_x$ (Me = W, Mo or V) catalyst towards methanol oxidation and their characterization. J Power Sources 2002;105:297-304.
29. Granqvist CG and Buhrman RA. Size distributions for supported metal catalysts: Coalescence growth versus Ostwald ripening. J Catal 1976;42:477-479.

30. Granqvist CG and Buhrman RA. Log-normal size distributions from magnetization measurements on small superconducting Al particles. J Appl Phys 1976;47:2200-2222.
31. Ehrburger P and Walker Jr. PR. Carbon as a support for catalysts:II. Size distribution of platinum particles on carbons of different heterogeneity before and after sintering. J Catal 1978;55:63-70.
32. Ribeiro J, dos Anjos DM, Leger J-M, Hahn F, Olivi P, de Andrade AR, Tremiliso-Filho G and Kokoh KB. Effect on W on PtSn/C catalysts for ethanol electrooxidation. J Appl Electrochem 2008;38:653-62.
33. Teran FE, Santos DM, Ribeiro J and Kokoh KB. Activity of PtSnRh/C nanoparticles for the electrooxidation of C1 and C2 alcohols. Thin Solid Films 2012;520:5846-5850.
34. Colmati F, Antolini E and Gonzalez ER. Preparation, structural characterization and activity for ethanol oxidation of carbon supported ternary Pt-Sn-Rh catalysts. J Alloys Compd 2008;456:264-270.
35. Hamnett A. Mechanism and electrocatalysis in the direct methanol fuel cell. Catal Today 1997;38:445-457.
36. Vielstich W. Electrochemical energy conversion – Methanol fuel cell as example. J Braz Chem Soc 2003;14:503-509.
37. Zhou WJ, Li WZ, Song SQ, Zhou ZH, Jiang LH, Sun GQ, Xin Q, Poulianitis K, Kontou S and Tsiakaras P. Bi- and tri-metallic Pt-based anode catalysts for direct ethanol fuel cells. J Power Sources 2004;131:217-223.
38. Cunha EM, Ribeiro J, Kokoh KB and de Andrade AR. Preparation, characterization and application of Pt-Ru-Sn/C trimetallic electrocatalysts for ethanol oxidation in direct fuel cell. Int J Hydrogen energy 2011;36:11034-11042.

*****